THE JOURNAL OF PHYSICAL CHEMISTRY LETTERS
A JOURNAL OF THE AMERICAN CHEMICAL SOCIETY

pubs.acs.org/JPCL

Letter

High-Speed Atomic Force Microscopy of the Structure and Dynamics of Calcite Nanoscale Etch Pits

Kazuki Miyata,* Kazuyoshi Takeuchi, Yuta Kawagoe, Peter Spijker, John Tracey, Adam S. Foster,* and Takeshi Fukuma*

Cite This: *J. Phys. Chem. Lett.* 2021, 12, 8039–8045

Read Online

ACCESS | Metrics & More | Article Recommendations | Supporting Information

ABSTRACT: Calcite dissolution is initiated by the formation of a nanoscale etch pit followed by step edge propagation and hence strongly influenced by the interactions between surface diffusing ions and step edges. However, such atomic-scale dynamics are mostly inaccessible with current imaging tools. Here, we overcome this limitation by using our recent development of high-speed frequency modulation atomic force microscopy. By visualizing atomic-scale structural changes of the etch pits at the calcite surface in water, we found the existence of mobile and less-mobile surface adsorption layers (SALs) in the etch pits. We also found that some etch pits maintain their size for a long time without expansion, and their step edges are often associated with less-mobile SALs, suggesting their step stabilization effect.

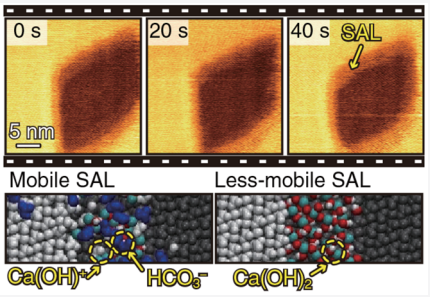

Calcite is one of the most abundant minerals in the earth, and its dissolution strongly affects the global environment. For example, it plays important roles in the global carbon cycle, influencing the concentration of carbon dioxide in the atmosphere and the pH of seawater.[1−4] In addition, calcite dissolution is related to the weathering of monuments and buildings,[5] land formation,[6] and biomineralization.[7,8] For predicting and controlling these phenomena, the mechanisms of calcite dissolution have been intensively studied both with experiments and simulations. In the experiments, macroscopic dissolution behaviors have been typically studied by monitoring the flow of material input to and output from a flow-through reactor,[9] while the microscopic or nanoscopic behaviors have been studied by atomic force microscopy (AFM),[10−12] optical interferometry,[13,14] transmission electron microscopy (TEM),[15] and X-ray reflection interface microscopy.[16] Alongside this, theoretical studies have been performed by molecular dynamics and kinetic Monte Carlo simulations using classical potentials or density functional theory.[14,17−21]

Calcite dissolution starts by the formation of a rhombic etch pit and progresses by the dissolution at its edges, leading to the propagation of the step edges.[22,23] Thus, the atomistic behaviors at step edges and inside of the etch pits can critically influence the kinetics of the dissolution. However, such atomistic phenomena have not been fully understood due to the difficulties in their direct visualization. For example, while previous experimental and theoretical studies suggested that the dissolution at the step edges may involve the dissociative adsorption of water, it has been difficult to directly confirm it by experiments.[10,21,24−27] In addition, the behavior of the ions desorbed from the step edges is also poorly understood. They may be directly desorbed from the step edges but can diffuse on the surfaces before desorption. Such surface diffusion processes should play an important role in the interaction between dissolving steps, especially at the edges of a small etch pit. However, the correlation between the surface diffusion of ions and the dissolution behavior of the step edges has not been understood in detail.

AFM was used earlier to visualize the nanoscale behaviors of the step edges and etch pits. Previous observations revealed the dependence of the step flow rate on the crystallographic orientation and pH.[28] Furthermore, the influence of impurities such as metal ions and organic additives on the shape and propagation of the step edges was also clarified by the AFM measurements.[7,29] However, it has been a great challenge to directly visualize atomic-scale structural changes at the step edges due to either insufficient spatial or temporal resolution. For example, high-speed amplitude modulation AFM (AM-AFM) was developed and successfully used for visualizing the dynamics of proteins as well as crystal growth and dissolution.[30−32] However, its spatial resolution has been limited to 1 nm. In the meantime, the development of the liquid-environment frequency modulation AFM (FM-AFM) enabled atomic-resolution imaging of various materials in a liquid.[33−35] However, its imaging speed was limited to 1 min/frame.

To overcome these limitations, we have recently developed high-speed FM-AFM and enabled atomic-resolution imaging

Received: June 29, 2021
Accepted: August 12, 2021
Published: August 17, 2021

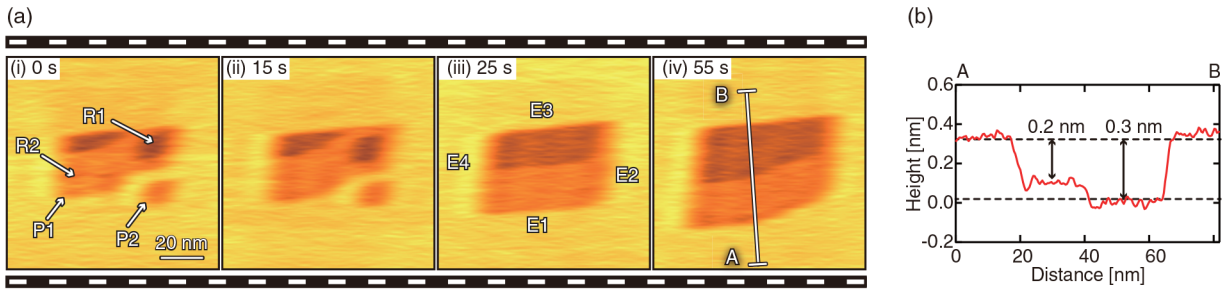

Figure 1. (a) Snapshots of successive FM-AFM images of the etch pits on the calcite $(10\bar{1}4)$ surface in water. Imaging speed: 5 s/frame. Scan size: 200 × 200 nm^2. Pixel size: 500 × 500 pix^2. E1 and E2 are obtuse steps. E3 and E4 are acute steps. (b) Height profile measured across line A−B.

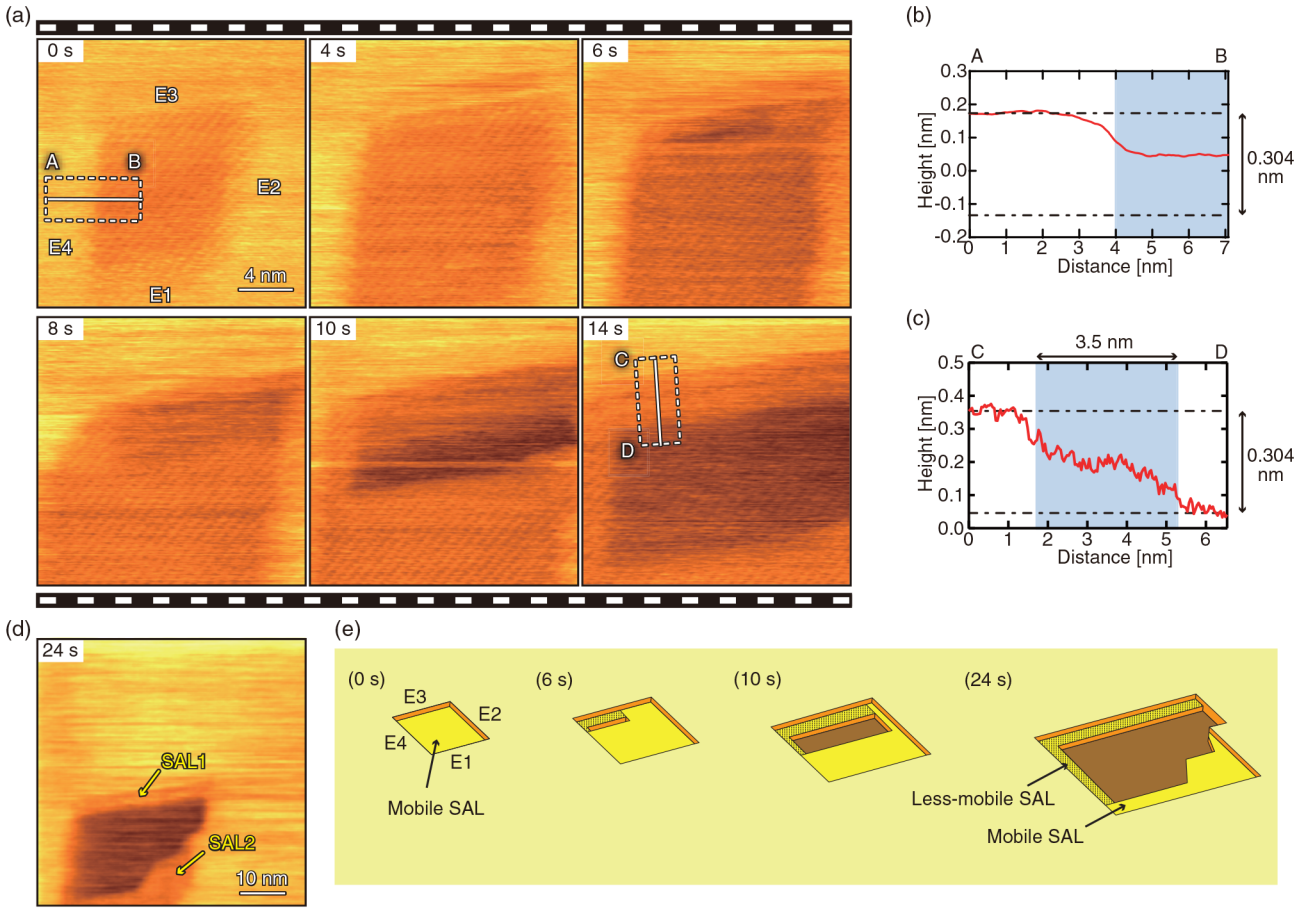

Figure 2. (a) Snapshots of successive FM-AFM images of the etch pits on the calcite $(10\bar{1}4)$ surface in water. Imaging speed: 2 s/frame. Scan size: 20 × 20 nm^2. Pixel size: 500 × 500 pix^2. E1 and E2 are obtuse steps. E3 and E4 are acute steps. (b, c) Height profiles measured along lines A−B and C−D, respectively. (d) FM-AFM image obtained immediately after the acquisition of (a). Imaging speed: 2 s/frame. Scan size: 60 × 60 nm^2. Pixel size: 500 × 500 pix^2. (e) Schematic model of each etch pits obtained in (a) and (d).

in liquid at 1 s/frame. With the developed system, we imaged atomic-scale structural changes at the step edges during dissolution in pure water and revealed the formation of a layer-like structure, referred to as the transition region (TR), along the step edges with an intermediate height between the upper and lower terraces and a width of a few nanometers.[36,37] In addition, our simulations suggested that the TR is most likely to be a $Ca(OH)_2$ monolayer formed as an intermediate state in the calcite dissolution. However, in these works, we failed to clarify the role of TR in the dissolution mechanism and the influence of the $CaOH^+$ and HCO_3^- on the interfacial structures and processes, despite them being obvious steps in the dissolution process. Furthermore, although the high-speed FM-AFM was previously used for the imaging of the isolated step edges, it has not been applied to the atomic-scale imaging of the nanoscale etch pits in spite of its importance in understanding the very initial stage of the calcite dissolution process.

In this study, we perform high-speed atomic-resolution FM-AFM imaging of nanoscale calcite etch pits in water. On the basis of the obtained images, we clarify dynamic changes in the atomistic structures formed near the step edges and inside the etch pits. In addition, we present important findings on the

https://doi.org/10.1021/acs.jpclett.1c02088
J. Phys. Chem. Lett. 2021, 12, 8039−8045

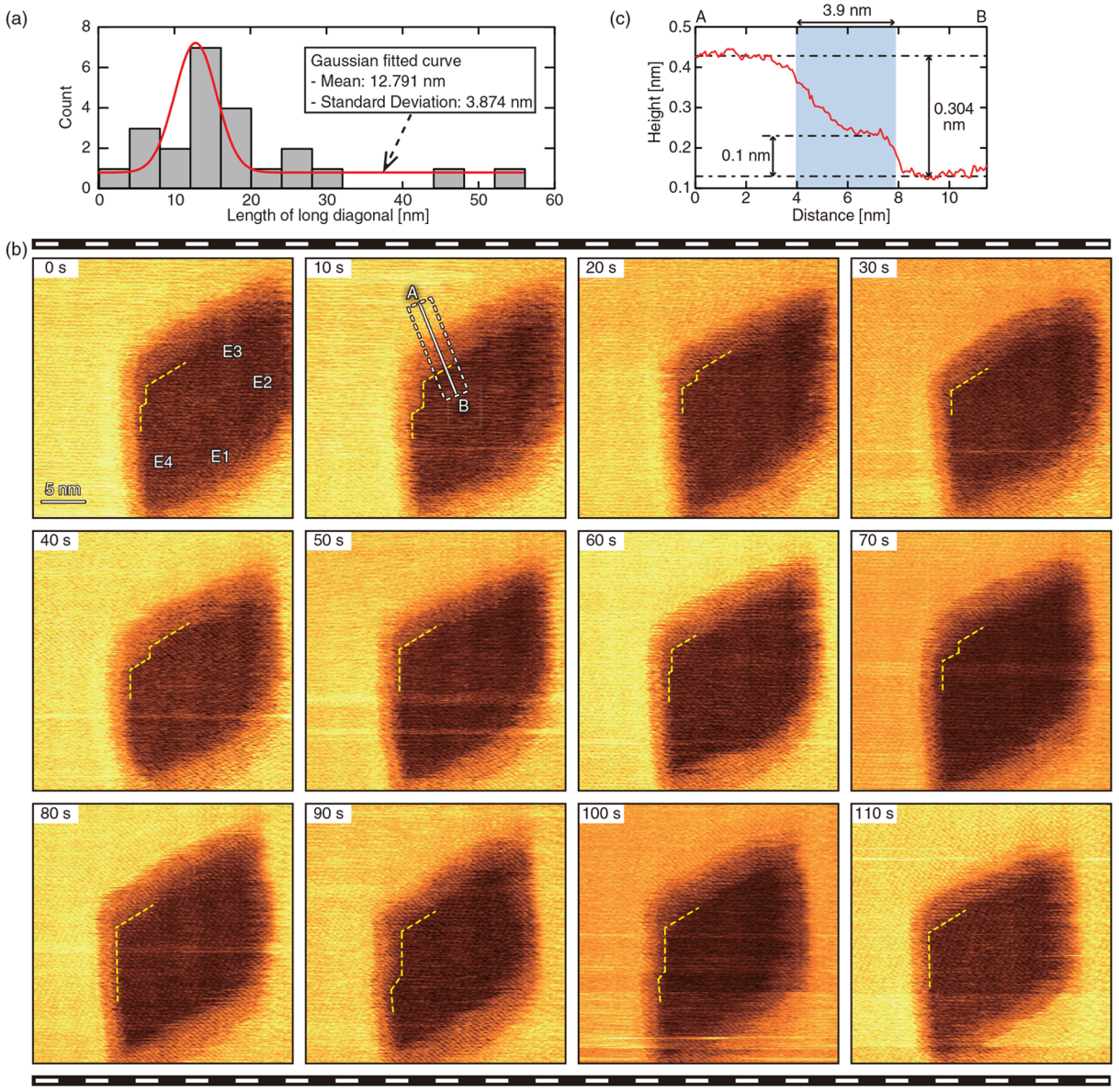

Figure 3. (a) Histogram of the long diagonal length distribution of the observed stable pits. (b) Snapshots of successive FM-AFM images of the etch pits on the calcite $(10\bar{1}4)$ surface in water. Imaging speed: 2 s/frame. Scan size: 30 × 30 nm^2. Pixel size: 500 × 500 pix^2. The yellow dotted line shows the form of the SAL in the upper left corner. E1 and E2 are obtuse steps. E3 and E4 are acute steps. (c) Height profile measured across line A−B.

correlation between the observed step edge structures and the dissolution mechanism.

Figure 1a shows snapshots of successive FM-AFM images of the etch pits on the calcite surface in pure water obtained at 5 s/frame. These images were obtained by applying a linear drift correction to the raw data and magnifying the same area around the etch pit. (See Movie 1 and Figure S1 for more details.) These images clearly show the dynamic structural changes of the nanoscale etch pits, demonstrating the capability of high-speed FM-AFM to visualize the initial stage of the crystal dissolution process.

At 0 s, two nanoscale etch pits are observed (P1 and P2). Among them, P1 shows two regions with different heights (R1 and R2). From 0 to 25 s, while P2 remains the same, P1 gradually expands to the lower direction in the image. From 15 to 25 s, P2 is merged into P1 to form a rhombic pit. Simultaneously, R1 and R2 dramatically changed their shape, and a layer with a constant width was formed along step edge E1. From 25 to 55 s, the etch pit shows anisotropic expansion. E2−E4 show almost no movement while E1 gradually moves downward in the image.

The height profile measured along line A−B (Figure 1b) shows that R1 is 0.3 nm lower than the upper terrace. This height corresponds to the single molecular step height of the calcite $(10\bar{1}4)$ surface (0.304 nm). R2 shows an intermediate height between the upper terrace and R1. Because of the dynamic changes of the R2 shape, it cannot be explained by a tip artifact. These results suggest that there are mobile species inside the etch pit and that they form a layer-like structure along a step edge. Hereafter, we refer to this layer-like structure as the surface adsorption layer (SAL).

https://doi.org/10.1021/acs.jpclett.1c02088
J. Phys. Chem. Lett. 2021, 12, 8039−8045

As discussed above, we previously found a similar layer-like structure, referred to as TR, formed along an "isolated" dissolving step edge as an intermediate state of dissolution.[36] However, our observation suggests that the SAL observed in Figure 1a is different from the TR. First, the width of TR is typically a few nanometers while that of the SAL can be as wide as 20 nm (Figure 1b). In addition, the width and shape of TR show little change during the dissolution while those of the SAL show significant changes.

A calcite $(10\bar{1}4)$ surface shows two types of molecular steps: acute and obtuse. They are known to show different step velocities during dissolution, with the obtuse steps dissolving faster than the acute steps. In Figure 1a, E1 moves much faster than the other edges. Since E1 is an obtuse step, it is reasonable that it moves much faster than E3 and E4 (i.e., acute steps). However, another obtuse step, E2, moves as slowly as the acute steps move, which cannot be explained by the dependence on the crystallographic direction.

In addition to the crystallographic orientation, it is likely that surface diffusing ions and adsorption layers formed at the step edges should also have a significant influence on the step dissolution rate, especially for small etch pits. To obtain further insights into the atomistic correlation between the step dissolution and surface adsorbed ions, we obtained successive FM-AFM images of a smaller etch pit with atomic-scale resolution as shown in Figure 2a. (See Movie 2 for more details.)

At 0 s, the image shows the rhombic etch pit surrounded by the four step edges E1−E4. The height profile A−B (Figure 2b) shows that the depth of the pit is much lower than the single molecular step height (∼0.3 nm). Thus, the pit should be filled with an SAL.

From 0 to 6 s, the pit expands mainly in the directions of step edges E1 and E2. At 6 s, a depression is created beside the tip near E3. After the formation of this depression, the pit starts to expand rapidly (from 6 to 14 s). However, E3 remains at almost the same position. When the rectangular depression is formed, a layer-like structure is formed along E3. The height profile C−D (Figure 2c) shows that this structure has a width of ∼3.5 nm. From 10 to 14 s, the width and the shape of this structure show little change.

To confirm the shape of the pits after expansion, a large area was scanned immediately after the acquisition of these successive images, as shown in Figure 2d. In this image, two SALs are observed along the step edges: SAL1 and SAL2. These two SALs have different structural and dynamic properties. SAL1 formed along E3 has a uniform width of a few nanometers and shows almost no structural changes. These features correspond well to those of a TR. In contrast, SAL2 formed along E1 and E2 has a nonuniform width of 2−10 nm and shows dynamic structural changes. These features are similar to those of the SAL observed in Figure 1a.

From these observations, we found that there are at least two types of SALs formed in a small pit: mobile and less-mobile SALs. On the basis of this finding, here we present a schematic model to explain the observed pit expansion process in Figure 2e. At 0 s, the pit was completely filled with an SAL. Upon the creation of a rectangular depression at 6 s, an SAL with a low mobility is formed along E3. From 6 to 24 s, the pit expands laterally. This expansion is mostly caused by the dissolution of E1 and E2, along with the formation of a high-mobility SAL. Meanwhile, E3 and E4, along which a less-mobile SAL is formed, show almost no displacement. These results, together with the results shown in Figure 1, consistently suggest that the less-mobile SAL may stabilize the step edges and prevent the pit expansion.

In this experiment, we found approximately 1 pit per a few μm^2 of surface area. Among the 63 pits observed in this study, we found that 23 of them (36.5%) maintain their shape and size for a relatively long time. This is unexpected because we performed experiments in pure water, where etch pits are supposed to expand rapidly. It is particularly surprising that even a relatively large pit (>50 nm) can maintain its shape without dissolution, as indicated by the size distribution of the observed stable pits (Figure 3a). Since it is impossible to see the moment of etch pit formation, it is difficult to accurately measure the stable period and to statistically analyze it. For the same reason, it is also difficult to confirm if such a period always exists after the pit formation. However, from the relatively large ratio of the stable pits (36.5%), we speculate that many of the pits are stabilized before they start to expand.

To investigate the mechanism stabilizing the pit structure, we observed atomic-scale structural changes at the step edges of a stable pit as shown in Figure 3b. (See Movie 3 for more details.) These images show that the rhombic shape and nanoscale size of the observed pit are largely maintained for more than ∼110 s.

Along the edges E1−E4, SALs with a width of a few nanometers are formed. Their apparent height is ∼0.1 nm as confirmed by the height profile in Figure 3c. These SALs seem to be relatively stable yet show minor structural changes as indicated by the yellow dotted lines in Figure 3b. This is probably due to the desorption and adsorption of the surface diffusing ions. Owing to the geometry and stability of the observed SAL, it is most likely to be a less-mobile SAL (i.e., TR). These results also support the hypothesis that the less-mobile SAL may stabilize the step edges.

To understand the species constituting the mobile and less-mobile SALs, the ions dissolved in the solution should be clarified. According to previous studies,[38] calcite dissolution in water involves the following chemical reactions:

$$CaCO_3 + H_2O \rightarrow CaOH^+ + HCO_3^- \quad (1)$$

$$CaOH^+ + HCO_3^- \rightarrow Ca(OH)_2 + CO_2 \quad (2)$$

$$Ca(OH)_2 \rightarrow Ca^{2+} + 2OH^- \quad (3)$$

$$HCO_3^- \rightleftharpoons H^+ + CO_3^{2-} \quad (4)$$

Thus, the ions and molecules on the right side of these formulas are candidates for the observed adsorbates to form the SALs.

In our previous study, we performed extensive MD simulations with various SAL models with different combinations of these ions and molecules. The obtained results revealed that in most of the models the adsorbates immediately form calcite or desorb from the surface, and only two models can stably form a layer-like structure along a step edge: models I and II in Figure 4. In these models, a monolayer depression is formed in the center of the periodic surface slab to create the upper and lower terraces. The adsorbates are placed along the left step edge to observe their stability. The snapshots shown in Figure 4 are taken 7.45 ns from the start of the simulation.

In model I, $CaOH^+$ and HCO_3^- ions produced by reaction 1 form an SAL, where a $CaOH^+$ monolayer is adsorbed on the lower terrace and its positive charge is compensated for by the

https://doi.org/10.1021/acs.jpclett.1c02088
J. Phys. Chem. Lett. 2021, 12, 8039−8045

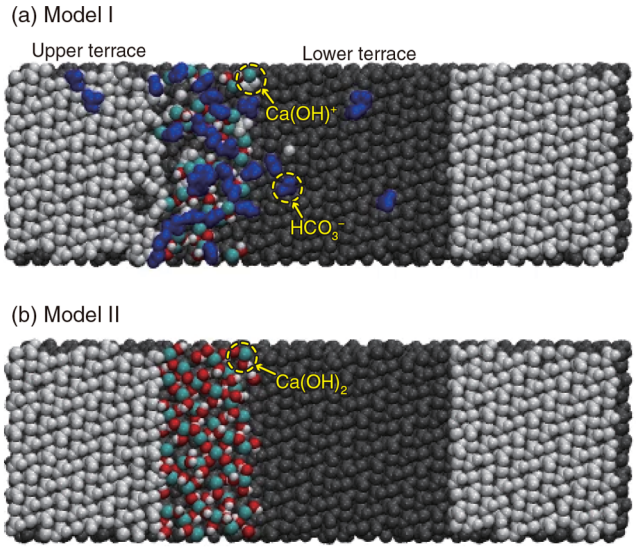

Figure 4. Snapshots of MD simulation models of the calcite $(10\bar{1}4)$ in water with (a) model I: $CaOH^+$ monolayer with diffusing HCO_3^- and (b) model II: $Ca(OH)_2$ monolayer. Snapshots were taken at 7.45 ns from the start.

HCO^- ions weakly adsorbed on it. Although $CaOH^+$ ions stay adsorbed in the proximity of the step edge, they are mobile enough to laterally diffuse. In model II, $Ca(OH)_2$ produced by reaction 2 forms an SAL, which corresponds to the TR reported in the previous studies.[36] In contrast to ions in model I, $Ca(OH)_2$ molecules show almost no lateral diffusion and are much less mobile. Therefore, the mobile and less-mobile SALs observed here most likely to correspond to models I and II, respectively.

In this study, we have performed high-speed FM-AFM imaging of nanoscale etch pits formed on the calcite $(10\bar{1}4)$ surfaces in water. The obtained images successfully visualized atomic-scale structural changes near the step edges in real time. From these images, we found that some of the small etch pits are surprisingly stable even in pure water, where calcite is supposed to dissolve. Inside of these small pits, two different types of SALs are found: the mobile and less-mobile SALs. The mobile SALs show dynamic changes in their shape, and the width measured from the step edge can be wider than several tens of nanometers. In contrast, the less-mobile SALs have a more uniform and narrower width of a few nanometers and show little change in their shape. These SALs show a strong correlation with the stabilities of the step edges constituting the etch pits. Namely, when the step edges of the etch pits are static, they are partially or wholly adjacent to the less-mobile SAL. When they are dissolving to expand the etch pits, they are mostly adjacent to the mobile SAL. These results strongly suggest that the formation of the less-mobile SAL can stabilize the step edges and hinder the expansion of the etch pits. In addition, we performed atomistic MD simulations of various SALs and found that only two types of SALs can stably exist along the step edges: models I and II. The simulation shows that in model I consisting of $CaOH^+$ and HCO_3^-, ions are much more mobile than model II consisting of $Ca(OH)_2$ molecules. Thus, it is likely that models I and II correspond to the observed mobile and less-mobile SALs, respectively. These findings of the structures and properties of SALs provide atomic-scale insights into the very initial stage of calcite dissolution.

The present study, together with the previous reports,[36,37] has demonstrated that high-speed FM-AFM is a powerful tool for investigating the atomic-scale mechanism of the calcite dissolution process. Although other applications of this technique have not yet been explored, it should be potentially useful for studying various other solid−liquid interfacial phenomena, including crystal growth and the dissolution of various materials, the self-assembly of organic and biological molecules, and structural changes associated with electrochemical reactions. The present work should stimulate such future studies in various scientific areas.

EXPERIMENTAL SECTION

In this study, we used a calcite substrate (Crystal Base Co, Ltd.) with a size of $5 \times 5 \times 2$ mm^3. The substrate was glued to the sample holder. Immediately after the cleavage of the substrate, 50 μL of Milli-Q water was dropped onto the sample surface. In the dropped water, we performed high-speed FM-AFM imaging in constant frequency shift mode at room temperature. For all experiments, we used the commercially available silicon cantilevers (AC55, Olympus), with a typical spring constant k, quality factor Q, and resonance frequency f_0 in an aqueous environment of 80 N/m and 10 and 1.5 MHz, respectively. To eliminate the contaminants on the tip surface, the tip was coated with a 15 nm silicon film by a dc sputter coater (K575XD, Emitech).[39] For high-speed FM-AFM operation with atomic-scale resolution, we used the custom-built FM-AFM setup with the low-noise cantilever deflection sensor,[40−42] highly stable photothermal cantilever excitation system,[42,43] high-speed scanner,[44] low-latency wideband PLL, and FM-AFM controller.[45] The use of a high-speed FM-AFM system was essential for the imaging of atomic-scale dynamics at the dissolving step edges. The detailed discussions on the required AFM imaging speed is given in the Supporting Information.

The detailed methods for the MD simulation were previously reported elsewhere.[46,47] Thus, here we describe them only briefly. All simulations were performed using the MD code LAMMPS,[48] and analysis was performed visually using VMD or numerically by the bespoke code using the Python library MD Analysis.[49,50] For this system, the same force field is used for the MD simulations as in the previous work.[36] In that work, we tested different setups with several species to investigate the origins of the TR and found calcium hydroxide to be the most likely model.

ASSOCIATED CONTENT

Supporting Information

The Supporting Information is available free of charge at https://pubs.acs.org/doi/10.1021/acs.jpclett.1c02088.

Discussions on drift correction for Figure 1 with supplementary figures S1 and AFM speed required for imaging atomic-scale dynamics around dissolving step edges (PDF)

Movie1.mp4: Successive FM-AFM images of calcite surface obtained in water, 5 s/frame; four images were selected and are shown in Figure 1a (MP4)

Movie2.mp4: Successive FM-AFM images of calcite surface obtained in water, 2 s/frame; six images were selected and shown in Figure 2a (MP4)

https://doi.org/10.1021/acs.jpclett.1c02088
J. Phys. Chem. Lett. 2021, 12, 8039−8045

Movie3.mp4: Successive FM-AFM images of calcite surface obtained in water, 2 s/frame; 12 images were selected and are shown in Figure 3b (MP4)

AUTHOR INFORMATION

Corresponding Authors

Kazuki Miyata − *Nano Life Science Institute (WPI-NanoLSI) and Division of Electrical Engineering and Computer Science, Kanazawa University, Kakuma-machi, Kanazawa 920-1192, Japan;* orcid.org/0000-0002-1641-2160; Email: k-miyata@staff.kanazawa-u.ac.jp

Adam S. Foster − *Nano Life Science Institute (WPI-NanoLSI), Kanazawa University, Kakuma-machi, Kanazawa 920-1192, Japan; Department of Applied Physics, Aalto University, Helsinki FI-00076, Finland;* orcid.org/0000-0001-5371-5905; Email: adam.foster@aalto.fi

Takeshi Fukuma − *Nano Life Science Institute (WPI-NanoLSI) and Division of Electrical Engineering and Computer Science, Kanazawa University, Kakuma-machi, Kanazawa 920-1192, Japan;* orcid.org/0000-0001-8971-6002; Email: fukuma@staff.kanazawa-u.ac.jp

Authors

Kazuyoshi Takeuchi − *Division of Electrical Engineering and Computer Science, Kanazawa University, Kakuma-machi, Kanazawa 920-1192, Japan*

Yuta Kawagoe − *Division of Electrical Engineering and Computer Science, Kanazawa University, Kakuma-machi, Kanazawa 920-1192, Japan*

Peter Spijker − *Department of Applied Physics, Aalto University, Helsinki FI-00076, Finland*

John Tracey − *Department of Applied Physics, Aalto University, Helsinki FI-00076, Finland*

Complete contact information is available at: https://pubs.acs.org/10.1021/acs.jpclett.1c02088

Notes

The authors declare no competing financial interest.

ACKNOWLEDGMENTS

This work was supported by World Premier International Research Center Initiative (WPI), MEXT, Japan and JSPS KAKENHI grant numbers JP20H00345, JP20H05212, and JP20K15172. Computing resources from the Aalto Science-IT project and CSC, Helsinki are gratefully acknowledged. A.S.F. was supported by the Academy of Finland (project no. 314862).

REFERENCES

(1) Reeder, R. J. In *Carbonates, Mineralogy, and Chemistry: Reviews in Mineralogy*; Reederi, R. J, Ed.; Mineralogical Society of America.

(2) Sigman, D. M.; Boyle, E. A. Glacial/Interglacial Variations in Atmospheric Carbon Dioxide. *Nature* **2000**, *407*, 859−869.

(3) Sarmiento, J.; Gruber, N. *Ocean Biogeochemical Dynamics*; Princeton University Press, 2006.

(4) Zeebe, R. E.; Zachos, J. C.; Caldeira, K.; Tyrrell, T. Carbon Emissions and Acidification. *Science* **2008**, *321*, 51−52.

(5) Moropoulou, A.; Bisbikou, K.; Torfs, K.; Grieken, R. V.; Zezza, F.; Macri, F. Origin and Growth of Weathering Crusts on Ancient Marbles in Industrial Atmosphere. *Atmos. Environ.* **1998**, *32*, 967−982.

(6) Borsato, A.; Frisia, S.; Jones, B.; van der Borg, K. Calcite Moonmilk: Crystal Morphology and Environment of Formation in Caves in the Italian Alps. *J. Sediment. Res.* **2000**, *70*, 1171−1182.

(7) Teng, H. H.; Dove, P. M. Surface Site-Specific Interactions of Aspartate with Calcite During Dissolution; Implications for Biomineralization. *Am. Mineral.* **1997**, *82*, 878−887.

(8) Sand, K. K.; Pedersen, C. S.; Sjöberg, S.; Nielsen, J. W.; Makovicky, E.; Stipp, S. L. S. Biomineralization: Long-Term Effectiveness of Polysaccharides on the Growth and Dissolution of Calcite. *Cryst. Growth Des.* **2014**, *14*, 5486−5494.

(9) Truesdale, V. W. Evidence and Potential Implications of Exponential Tails to Concentration Versus Time Plots for the Batch Dissolution of Calcite. *Aquat. Geochem.* **2015**, *21*, 365−396.

(10) Shiraki, R.; Rock, P. A.; Casey, W. Dissolution Kinetics of Calcite in 0.1 M NaCl Solution at Room Temperature: An Atomic Force Microscopic (AFM) Study. *Aquat. Geochem.* **2000**, *6*, 87−108.

(11) Hillner, P. E.; Gratz, A. J.; Manne, S.; Hansma, P. K. Atomic-Scale Imaging of Calcite Growth and Dissolution in Real Time. *Geology* **1992**, *20*, 359−362.

(12) Stipp, S. L. S.; Eggleston, C. M.; Nielssen, B. S. Calcite Surface Structure Observed at Microtopographic and Molecular Scales with Atomic Force Microscopy (AFM). *Geochim. Cosmochim. Acta* **1994**, *58*, 3023−3033.

(13) Arvidson, R. S.; Ertan, I. E.; Amonette, J. E.; Luttge, A. Variation in Calcite Dissolution Rates:A Fundamental Problem. *Geochim. Cosmochim. Acta* **2003**, *67*, 1623−1634.

(14) Lasaga, A. C.; Luttge, A. Variation of Crystal Dissolution Rate Based on a Dissolution Stepwave Model. *Science* **2001**, *291*, 2400−2404.

(15) Nielsen, M. H.; Aloni, S.; Yoreo, J. J. D. In Situ TEM Imaging of $CaCO_3$ Nucleation Reveals Coexistence of Direct and Indirect Pathways. *Science* **2014**, *345*, 1158−1162.

(16) Clark, J. N.; Ihli, J.; Schenk, A. S.; Kim, Y.-Y.; Kulak, A. N.; Campbell, J. M.; Nisbet, G.; Meldrum, F.; Robinson, I. K. Three-dimensional Imaging of Dislocation Propagation During Crystal Growth and Dissolution. *Nat. Mater.* **2015**, *14*, 780−784.

(17) Spagnoli, D.; Kerisit, S.; Parker, S. C. Atomistic Simulation of the Free Energies of Dissolution of Ions from Flat and Stepped Calcite Surfaces. *J. Cryst. Growth* **2006**, *294*, 103−110.

(18) de la Pierre, M.; Raiteri, P.; Gale, J. D. Structure and Dynamics of Water at Step Edges on the Calcite $\{10\bar{1}4\}$ Surface. *Cryst. Growth Des.* **2016**, *16*, 5907−5914.

(19) McCoy, J. M.; LaFemina, J. P. Kinetic Monte Carlo Investigation of Pit Formation at the $CaCO_3$ $(10\bar{1}4)$ Surface-Water Interface. *Surf. Sci.* **1997**, *373*, 288−299.

(20) Kurganskaya, I.; Luttge, A. Kinetic Monte Carlo Approach To Study Carbonate Dissolution. *J. Phys. Chem. C* **2016**, *120*, 6482−6492.

(21) Lardge, J. S.; Duffy, D. M.; Gillan, M. J.; Watkins, M. Ab Initio Simulations of the Interaction between Water and Defects on the Calcite $(10\bar{1}4)$ Surface. *J. Phys. Chem. C* **2010**, *114*, 2664−2668.

(22) Liang, Y.; Baer, D. R.; McCoy, J. M.; Amonette, J. E.; Lafemina, J. P. Dissolution Kinetics at the Calcite-water Interface. *Geochim. Cosmochim. Acta* **1996**, *60*, 4883−4887.

(23) Jordan, G.; Rammensee, W. Dissolution Rates of Calcite $(10\bar{1}4)$ Obtained by Scanning Force Microscopy: Microtopography-Based Dissolution Kinetics on Surfaces with Anisotropic Step Velocities. *Geochim. Cosmochim. Acta* **1998**, *62*, 941−947.

(24) Neagle, W.; Rochester, C. H. Infrared Study of the Adsorption of Water and Ammonia on Calcium Carbonate. *J. Chem. Soc., Faraday Trans.* **1990**, *86*, 181−183.

(25) Kuriyavar, S. I.; Vetrivel, R.; Hegde, S. G.; Ramaswamy, A. V.; Chakrabarty, D.; Mahapatra, S. Insights into the Formation of Hydroxyl Ions in Calcium Carbonate: Temperature Dependent FTIR and Molecular Modelling Studies. *J. Mater. Chem.* **2000**, *10*, 1835−1840.

(26) Stipp, S. L.; Hochella, M. F. Structure and Bonding Environments at the Calcite Surface as Observed with X-ray Photoelectron Spectroscopy (XPS) and Low Energy Electron Diffraction (LEED). *Geochim. Cosmochim. Acta* **1991**, *55*, 1723−1736.

(27) Kerisit, S.; Parker, S. C.; Harding, J. H. Atomistic Simulation of the Dissociative Adsorption of Water on Calcite Surfaces. *J. Phys. Chem. B* **2003**, *107*, 7676−7682.
(28) De Giudici, G. Surface Control Vs. Diffusion Control During Calcite Dissolution: Dependence of Step-Edge Velocity upon Solution pH. *Am. Mineral.* **2002**, *87*, 1279−1285.
(29) Lea, A. S.; Amonette, J. E.; Baer, D. R.; Liang, Y.; Colton, N. G. Microscopic Effects of Carbonate, Manganese, and Strontium Ions on Calcite Dissolution. *Geochim. Cosmochim. Acta* **2001**, *65*, 369−379.
(30) Kodera, N.; Yamamoto, D.; Ishikawa, R.; Ando, T. Video Imaging of Walking Myosin V by High-Speed Atomic Force Microscopy. *Nature* **2010**, *468*, 72−76.
(31) Paloczi, G. T.; Smith, B. L.; Hansma, P. K.; Walters, D. A.; Wendman, M. A. Rapid Imaging of Calcite Crystal Growth Using Atomic Force Microscopy with Small Cantilevers. *Appl. Phys. Lett.* **1998**, *73*, 1658−1660.
(32) Bozchalooi, I. S.; Houck, A. C.; AlGhamdi, J. M.; Youcef-Toumi, K. Design and Control of Multi-actuated Atomic Force Microscope for Large-range and High-speed Imaging. *Ultramicroscopy* **2016**, *160*, 213−224.
(33) Fukuma, T.; Kobayashi, K.; Matsushige, K.; Yamada, H. True Atomic Resolution in Liquid by Frequency-Modulation Atomic Force Microscopy. *Appl. Phys. Lett.* **2005**, *87*, 034101.
(34) Rode, S.; Oyabu, N.; Kobayashi, K.; Yamada, H.; Kühnle, A. True Atomic-Resolution Imaging of (10$\bar{1}$4) Calcite in Aqueous Solution by Frequency Modulation Atomic Force Microscopy. *Langmuir* **2009**, *25*, 2850−2853.
(35) Kobayashi, N.; Itakura, S.; Asakawa, H.; Fukuma, T. Atomic-Scale Processes at the Fluorite-Water Interface Visualized by Frequency Modulation Atomic Force Microscopy. *J. Phys. Chem. C* **2013**, *117*, 24388−24396.
(36) Miyata, K.; Tracey, J.; Miyazawa, K.; Haapasilta, V.; Spijker, P.; Kawagoe, Y.; Foster, A. S.; Tsukamoto, K.; Fukuma, T. Dissolution Processes at Step Edges of Calcite in Water Investigated by High-Speed Frequency Modulation Atomic Force Microscopy and Simulation. *Nano Lett.* **2017**, *17*, 4083−4089.
(37) Miyata, K.; Kawagoe, Y.; Tracey, J.; Miyazawa, K.; Foster, A. S.; Fukuma, T. Variations in Atomic-Scale Step Edge Structures and Dynamics of Dissolving Calcite in Water Revealed by High-Speed Frequency Modulation Atomic Force Microscopy. *J. Phys. Chem. C* **2019**, *123*, 19786−19793.
(38) Van Cappellen, P.; Charlet, L.; Stumm, W.; Wersin, P. A Surface Complexation Model of the Carbonate Mineral-aqueous Solution. *Geochim. Cosmochim. Acta* **1993**, *57*, 3505−3518.
(39) Akrami, S. M. R.; Nakayachi, H.; Watanabe-Nakayama, T.; Asakawa, H.; Fukuma, T. Significant Improvements in Stability and Reproducibility of Atomic-Scale Atomic Force Microscopy in Liquid. *Nanotechnology* **2014**, *25*, 455701.
(40) Fukuma, T.; Kimura, M.; Kobayashi, K.; Matsushige, K.; Yamada, H. Development of Low Noise Cantilever Deflection Sensor for Multienvironment Frequency-Modulation Atomic Force Microscopy. *Rev. Sci. Instrum.* **2005**, *76*, 053704.
(41) Fukuma, T.; Jarvis, S. P. Development of Liquid-Environment Frequency Modulation Atomic Force Microscope with Low Noise Deflection Sensor for Cantilevers of Various Dimensions. *Rev. Sci. Instrum.* **2006**, *77*, 043701.
(42) Fukuma, T. Wideband Low-Noise Optical Beam Deflection Sensor with Photothermal Excitation for Liquid-Environment Atomic Force Microscopy. *Rev. Sci. Instrum.* **2009**, *80*, 023707.
(43) Fukuma, T.; Onishi, K.; Kobayashi, N.; Matsuki, A.; Asakawa, H. Atomic-Resolution Imaging in Liquid by Frequency Modulation Atomic Force Microscopy Using Small Cantilevers with Megahertz-Order Resonance Frequencies. *Nanotechnology* **2012**, *23*, 135706.
(44) Miyata, K.; Usho, S.; Yamada, S.; Furuya, S.; Yoshida, K.; Asakawa, H.; Fukuma, T. Separate-Type Scanner and Wideband High-Voltage Amplifier for Atomic-Resolution and High-Speed Atomic Force Microscopy. *Rev. Sci. Instrum.* **2013**, *84*, 043705.
(45) Miyata, K.; Fukuma, T. Quantitative Comparison of Wideband Low-Latency Phase-Locked Loop Circuit Designs for High-Speed Frequency Modulation Atomic Force Microscopy. *Beilstein J. Nanotechnol.* **2018**, *9*, 1844−1855.
(46) Fukuma, T.; Reischl, B.; Kobayashi, N.; Spijker, P.; Canova, F. F.; Miyazawa, K.; Foster, A. S. Mechanism of Atomic Force Microscopy Imaging of Three-Dimensional Hydration Structures at a Solid-Liquid Interface. *Phys. Rev. B: Condens. Matter Mater. Phys.* **2015**, *92*, 155412.
(47) Reischl, B.; Watkins, M.; Foster, S. A. Free Energy Approaches for Modeling Atomic Force Microscopy in Liquids. *J. Chem. Theory Comput.* **2013**, *9*, 600−608.
(48) Plimpton, S. Fast Parallel Algorithms for Short-Range Molecular. *J. Comput. Phys.* **1995**, *117*, 1−19.
(49) Humphrey, W.; Dalke, A.; Schulten, K. VMD: Visual Molecular Dynamics. *J. Mol. Graphics* **1996**, *14*, 33−38.
(50) Michaud-Agrawal, N.; Denning, E. J.; Woolf, T. B.; Beckstein, O. MDAnalysis: A Toolkit for the Analysis of Molecular Dynamics Simulations. *J. Comput. Chem.* **2011**, *32*, 2319−2327.

https://doi.org/10.1021/acs.jpclett.1c02088
J. Phys. Chem. Lett. 2021, 12, 8039−8045